INTERNATIONAL JOURNAL FOR NUMERICAL METHODS IN FLUIDS
Int. J. Numer. Meth. Fluids 2016; **80**:429–450
Published online 8 September 2015 in Wiley Online Library (wileyonlinelibrary.com). DOI: 10.1002/fld.4087

Two-level consistent splitting methods based on three corrections for the time-dependent Navier–Stokes equations

Qingfang Liu[1,2,*,†], Yanren Hou[1,2], Zhiheng Wang[3] and Jiakun Zhao[1]

[1]*School of Mathematics and Statistics, Xi'an Jiaotong University, Xi'an 710049, China*
[2]*Center for Computational Geosciences, Xi'an Jiaotong University, Xi'an 710049, China*
[3]*School of Energy Power Engineering, Xi'an Jiaotong University, Xi'an 710049, China*

SUMMARY

Three kinds of two-level consistent splitting algorithms for the time-dependent Navier–Stokes equations are discussed. The basic technique of two-level type methods for solving the nonlinear problem is first to solve a nonlinear problem in a coarse-level subspace, then to solve a linear equation in a fine-level subspace. Hence, the two-level methods can save a lot of work compared with the one-level methods. The approaches to linearization are considered based on Stokes, Newton, and Oseen corrections. The stability and convergence demonstrate that the two-level methods can acquire the optimal accuracy with the proper choice of the coarse and fine mesh scales. Numerical examples show that Stokes correction is the simplest, Newton correction has the best accuracy, while Oseen correction is preferable for the large Reynolds number problems and the long-time simulations among the three methods. Copyright © 2015 John Wiley & Sons, Ltd.

Received 22 June 2015; Accepted 19 July 2015

KEY WORDS: two-level methods; consistent splitting scheme; Navier–Stokes equations; stability; error estimates

1. INTRODUCTION

In this article, we consider the following incompressible time-dependent Navier–Stokes equations

$$\begin{cases} u_t - \nu\Delta u + (u\cdot\nabla)u + \nabla p = f \ \ \forall (x,t)\in\Omega\times[0,T], \\ \nabla\cdot u = 0 \ \ \forall (x,t)\in\Omega\times[0,T], \\ u = 0 \ \ \forall t\in[0,T], \forall x\in\partial\Omega, \\ u(x,0) = u_0 \ \ \forall x\in\Omega. \end{cases} \tag{1.1}$$

Let Ω be a bounded domain in $\mathbb{R}^d\,(d=2,3)$ and assumed to have a Lipschitz continuous boundary, u is the velocity field, u_0 is the initial velocity satisfying $\nabla\cdot u_0 = 0$, p denotes the pressure, f is the density of body forces, $\nu > 0$ is the kinetic viscosity, and $T > 0$ denotes a finite time.

It is well known that the coupling of the velocity and the pressure encounters a main difficulty for solving the incompressible Navier–Stokes equations numerically. To decouple the velocity and the pressure, Chorin [1] and Temam [2] originally introduced the projection type methods in the 1960s in which a provisional velocity is used to acquire the velocity and the pressure independently. Later on, many articles have been proposed to discuss the various projection methods. For example, the pressure-correction schemes [1, 2], velocity-correction schemes [3], and the consistent splitting schemes [4]. In order to decouple the velocity and the pressure, the pressure-correction schemes and the velocity-correction schemes impose a non-physical boundary condition on the pressure,

*Correspondence to: Qingfang Liu, Mathematics, Xi'an Jiaotong University, Xi'an 710049, China.
†E-mail: qfliu2010@mail.xjtu.edu.cn

which limits the accuracy of the pressure [5]. Unlike the pressure-correction and velocity-correction schemes, analysis and numerical examples show that the consistent splitting schemes can reach the optimal convergence rate (see the numerical tests in [4] and the analysis in [6]). At every time step, the consistent splitting schemes include the following two steps:

- Step 1: Acquire the velocity by solving a fully nonlinear equation,
- Step 2: Acquire the pressure by solving a Possion equation.

At the aforementioned Step 1, the existing consistent splitting schemes replace the nonlinear terms $u\cdot\nabla u$ by the value of last time step to avoid solving a fully nonlinear equation [3, 4], that is to say, the explicit scheme. However, the explicit scheme requires smaller time step than the implicit scheme. The fully implicit scheme is stable unconditionally in some sense, but it requires solving a nonlinear equation at each time step. A fully implicit treatment on the nonlinear term based on the two-level methods is considered in this paper. The two-level methods are the alternative choice for solving the nonlinear PDEs effectively. For examples, Xu *et al.* [7–9] apply the two-level techniques for solving the general linear and nonlinear PDEs, Stokes/Darcy, and Navier–Stokes/Darcy problems. The two-level methods for the Navier–Stokes equations have been discussed by Layton [10], Novo *et al.* [11, 12], Hou *et al.* [13–19], He *et al.* [20–22], and Shang *et al.* [23, 24].

The basic idea of the two-level type methods for solving the nonlinear equation is first to solve a nonlinear equation to acquire the large eddy components (u_H, p_H) in a coarse-level subspace and then solve a linear equation in a fine-level subspace to acquire the fine-level approximation (u_h, p_h). In fact, we can decompose (u_h, p_h) as $(u_h, p_h) = (u_H, p_H) + (\hat{u}_H, \hat{p}_H)$, where (u_H, p_H) is called the large eddy components and $(\hat{u}_H, \hat{p}_H)$ is called the small eddy components. In the two-level methods, the linear equation reflects the interactive relation between large eddy components (u_H, p_H) and small eddy components $(\hat{u}_H, \hat{p}_H)$, which plays an important role in the effectiveness of the two-level methods. Recently, some articles have been reported to discuss the two-level iterative methods for the steady Navier–Stokes equations. For examples, He *et al.* [21, 22] study some two-level iterative FEMs for the steady Navier–Stokes equations. Shang *et al.* [23, 24] combine the two-level method with the subgrid stabilized method and the local and parallel FEMs, respectively, for the steady Navier–Stokes equations. However, to our knowledge, there are few articles discussing the comparison of different interactive relations between large and small eddy components for the time-dependent Navier–Stokes equations. The interactive relation between large and small eddy components for the time-dependent Navier–Stokes equations should be more complicated compared with the case for the steady Navier–Stokes equations because the time term is involved. This paper combine the two-level method with the consistent splitting schemes for solving the time-dependent Navier–Stokes equations. We consider three kinds of two-level consistent splitting algorithms for the time-dependent Navier–Stokes equations. This paper can be viewed as a sequel to the work of Liu *et al.* [17, 18] and He *et al.* [22–24]. Among the discussed three algorithms, although two algorithms (labeled as Stokes correction and Newton correction algorithms) were developed in previous papers [17, 18], a new algorithm (labeled as Oseen correction algorithm) is developed in this paper. For the steady Navier–Stokes equations, Oseen correction algorithm is preferable for the small viscosity [22]. For the time-dependent Navier–Stokes equations, numerical analysis and numerical examples in this article show that Oseen correction algorithm is preferable for the small viscosity problem and the long-time simulations.

This paper is arranged as follows: Section 2 gives some mathematical preliminaries. Section 3 gives the three kinds of two-level consistent splitting schemes. In Section 4, we present some numerical examples. Finally, we give the conclusions in Section 5.

2. PRELIMINARIES

We introduce the following Hilbert spaces:

$$X = H_0^1(\Omega)^d, \quad Y = L^2(\Omega)^d, \quad M = L_0^2(\Omega) = \left\{ q \in L^2(\Omega); \int_\Omega q \mathrm{d}x = 0 \right\}.$$

DOI: 10.1002/fld

We denote the bilinear form $a(\cdot,\cdot)$ on $X\times X$ and trilinear form $b(\cdot,\cdot,\cdot)$ on $X\times X\times X$ respectively by

$$\begin{aligned} a(u,v) &=< Au, v >_{X'} = ((u,v)), \quad \forall u,v\in X,\\ b(u,v,w) &=< B(u,v), w >_{X'} = ((u\cdot\nabla)v,w) + \frac{1}{2}((\nabla\cdot u)v,w)\\ &= \frac{1}{2}((u\cdot\nabla)v,w) - \frac{1}{2}((u\cdot\nabla)w,v), \quad \forall u,v,w\in X, \end{aligned}$$

where $A=-P\Delta$, $B=P(u\cdot\nabla u)$, where P is the orthogonal projection of Y onto the divergence-free space.

Based on the aforementioned notations, the variational form of the Navier–Stokes equations (1.1) is to find $(u,p)\in(X,M)$ such that

$$\begin{aligned} &(u_t,v)+\nu a(u,v)+b(u,u,v)+(v,\nabla p)=(f,v), \quad \forall v\in X,\\ &(\nabla\cdot u,q)=0, \quad \forall q\in M. \end{aligned} \tag{2.1}$$

In the following text, we need the regularity of the exact solution of the Navier–Stokes equations [25].

Theorem 2.1
Assume that $f_{tt}\in L^\infty(0,T;H)$; then there exists a positive constant κ such that

$$\|u(t)\|_2+\|u_{tt}(t)\|_0+\|p(t)\|_1+\|p_{tt}(t)\|_0\leqslant\kappa \quad \forall t\in[0,T].$$

In the following text, we use c to denote a common constant and κ to denote a constant, which may depend additionally on ν, u_0 and on time t, assumed to be continuous with respect to t. We denote by T a positive constant satisfying $0\leqslant T\leqslant+\infty$ for $d=2$ and $0\leqslant T<T^*$ for $d=3$, where T^* denotes the length of the time interval on which the strong solution exists.

To end this section, we recall some inequalities that are useful in the following analysis [20, 26].

$$b(u_h,v_h,w_h)=-b(u_h,w_h,v_h), \tag{2.2}$$

$$\begin{aligned} |b(u_h,v_h,w_h)| &\leqslant c_0\|u_h\|_{1+s}\|v_h\|_1\|w_h\|_0, c_0\|u_h\|_1\|v_h\|_{1+s}\|w_h\|_0,\\ &c_0\|u_h\|_0\|v_h\|_{1+s}\|w_h\|_1, \quad \forall s>1, \end{aligned} \tag{2.3}$$

$$|b(u_h,v_h,w_h)|\leqslant c_0(\|u_h\|_0\|v_h\|_1+\|u_h\|_1\|v_h\|_0)\|w_h\|_{L^\infty}, \tag{2.4}$$

for $\forall u_h,v_h,w_h\in X_h$, and c_0 is a constant depending only on Ω.

We have the Brezis–Gallouet inequality in the finite dimensional case [27],

$$\|u_h\|_{L^\infty}\leqslant cL_h\|\nabla u_h\|_0, \quad \forall u_h\in X_h, \tag{2.5}$$

where $L_h=|\log(h)|^{\frac{1}{2}}$ for $d=2$ and $L_h=h^{-\frac{1}{2}}$ for $d=3$.

3. TWO-LEVEL CONSISTENT SPLITTING SCHEMES

In this section, we discuss some two-level consistent splitting methods for the time-dependent Navier–Stokes equations and their stability and convergence results. For the space discretization, we use FEMs. Specially, let h be a real positive parameter tending to 0. The finite element subspace (X_h,M_h) is characterized by τ_h, which is a partition of Ω into triangles K or quadrilaterals K, assumed to be uniformly regular as h tending to 0.

Let $P_h: X\to X_h$ be the orthogonal projection defined by

$$(v-P_hv,v_h)=0, \quad \forall v\in X, \quad \forall v_h\in X_h.$$

DOI: 10.1002/fld

Furthermore, the projection P_h satisfies the following properties [20, 25].

$$\begin{aligned} &\|P_h v\|_0 \leqslant c\|v\|_0, \quad \forall v \in X, \\ &\|v - P_h v\|_0 + h\|v - P_h v\|_1 \leqslant ch^2\|Av\|_0, \quad \forall v \in H^2(\Omega)^d. \end{aligned} \tag{3.1}$$

3.1. Two-level consistent splitting scheme based on Stokes correction

Firstly, we introduce the two-level consistent splitting methods of (1.1) based on Stokes correction. We call it Method I. Let $u_h^0 = P_h u_0$, $u_H^0 = P_H u_0$ and positive integer $n(0 \leqslant n \leqslant N = T/k)$. Method I is achieved by the following three steps:

Step 1. Find a coarse-level solution $(u_H^{n+1}, p_H^{n+1}) \in (X_H, M_H)$ such that

$$\left(d_t u_H^{n+1}, v\right) + \nu a\left(u_H^{n+1}, v\right) + b\left(u_H^{n+1}, u_H^{n+1}, v\right) + \left(v, \nabla p_H^{n+1}\right) - \left(u_H^{n+1}, \nabla q\right) = \left(f^{n+1}, v\right), \tag{3.2}$$

for all $(v, q) \in (X_H, M_H)$. Here, k is the time step length, and $d_t u_H^{n+1} = \frac{1}{k}(u_H^{n+1} - u_H^n)$, $f^{n+1} = f(t_{n+1})$, $t_n = nk$.

Step 2a. Find a fine-level solution $u_h^{n+1} \in X_h$ defined by the following Stokes problem:

$$\left(d_t u_h^{n+1}, v\right) + \nu a\left(u_h^{n+1}, v\right) + b\left(u_H^{n+1}, u_H^{n+1}, v\right) + \left(v, \nabla p_h^n\right) = \left(f^{n+1}, v\right), \quad \forall v \in X_h.$$

Step 3. Update $p_h^{n+1} \in M_h$ defined by

$$\left(\nabla\left(p_h^{n+1} - p_h^n + \nu\nabla \cdot u_h^{n+1}\right), \nabla q\right) = \left(d_t u_h^{n+1}, \nabla q\right), \quad \forall q \in M_h. \tag{3.3}$$

The following theorems provide the stability and convergence results of Method I [17].

Theorem 3.1
Suppose that $0 < k < c$. Then the solution of Method I has the following estimates:

$$\|u_h^n\|_0^2 + k\nu \sum_{i=0}^{n} \left(\|\nabla u_h^i\|_0^2 + \|p_h^i\|_0^2\right) \leqslant \kappa, \quad 0 \leqslant n \leqslant N.$$

Theorem 3.2
Under the conditions of Theorem 2.1 and Theorem 3.1, we have

$$\|u(t_n) - u_h^n\|_0^2 + k\nu \sum_{i=0}^{n} \left(\|\nabla u(t_i) - \nabla u_h^i\|_0^2 + \|p(t_i) - p_h^i\|_0^2\right) \leqslant \kappa\left(H^6 L_h^2 + h^4 + k^2\right), \quad 0 \leqslant n \leqslant N.$$

3.2. Two-level consistent splitting scheme based on Newton correction

Secondly, we introduce the two-level consistent splitting methods of (1.1) based on Newton correction. We call it Method II, which is achieved by the following three steps:

Step 1. Find a coarse-level solution $(u_H^{n+1}, p_H^{n+1}) \in (X_H, M_H)$ defined by (3.2).

Step 2b. Find a fine-level solution $u_h^{n+1} \in X_h$ defined by the following problem:

$$\begin{aligned} &\left(d_t u_h^{n+1}, v\right) + \nu a\left(u_h^{n+1}, v\right) + b\left(u_H^{n+1}, u_h^{n+1}, v\right) + b\left(u_h^{n+1}, u_H^{n+1}, v\right) + \left(v, \nabla p_h^n\right) \\ &= \left(f^{n+1}, v\right) + b\left(u_H^{n+1}, u_H^{n+1}, v\right), \quad \forall v \in X_h. \end{aligned}$$

Step 3. Update $p_h^{n+1} \in M_h$ defined by (3.3).

In our recent paper [18], we have the following estimates of Method II.

DOI: 10.1002/fld

Theorem 3.3
Under the conditions of Theorem 3.1, the solution of Method II has the following estimates:

$$\|u_h^n\|_0^2 + k\nu \sum_{i=0}^{n} \left(\|\nabla u_h^i\|_0^2 + \|p_h^i\|_0^2\right) \leqslant \kappa, \quad 0 \leqslant n \leqslant N.$$

Theorem 3.4
Under the conditions of Theorem 3.2, we have

$$\|u(t_n) - u_h^n\|_0^2 + k\nu \sum_{i=0}^{n} \left(\|\nabla u(t_i) - \nabla u_h^i\|_0^2 + \|p(t_i) - p_h^i\|_0^2\right) \leqslant \kappa \left(H^8 L_h^2 + h^4 + k^2\right), \quad 0 \leqslant n \leqslant N.$$

3.3. Two-level consistent splitting scheme based on Oseen correction

Finally, we introduce the two-level consistent splitting methods of (1.1) based on Oseen correction. We call it Method III, which is achieved by the following three steps:

Step 1. Find a coarse-level solution $(u_H^{n+1}, p_H^{n+1}) \in (X_H, M_H)$ defined by (3.2).
Step 2c. Find a fine-level solution $u_h^{n+1} \in X_h$ defined by the following Oseen problem:

$$\left(d_t u_h^{n+1}, v\right) + \nu a\left(u_h^{n+1}, v\right) + b\left(u_H^{n+1}, u_h^{n+1}, v\right) + \left(v, \nabla p_h^n\right) = \left(f^{n+1}, v\right), \quad \forall v \in X_h. \tag{3.4}$$

Step 3. Update $p_h^{n+1} \in X_h$ defined by (3.3).

In the following text, we give a detailed analysis of the stability and convergence of Method III. Before giving the stability results, we first show a discrete Gronwall lemma provided in [26, 28].

Lemma 3.1
Let k, C, and a_n, b_n, c_n, d_n for integers $n \geqslant 0$ be nonnegative number such that

$$a_m + k\sum_{n=1}^{m} b_n \leqslant k\sum_{n=1}^{m} d_n a_n + k\sum_{n=1}^{m} c_n + C, \quad \forall m \geqslant 1.$$

Suppose that $kd_n < 1$ for all n, and set $\gamma_n = (1 - kd_n)^{-1}$. Then,

$$a_m + k\sum_{n=1}^{m} b_n \leqslant \exp\left(k\sum_{n=1}^{m} \gamma_n d_n\right)\left(k\sum_{n=1}^{m} c_n + C\right), \quad \forall m \geqslant 1.$$

In the following text, we obtain the stability of Method III. We first have the following lemma.

Lemma 3.2
Under the conditions of Theorem 2.1, there exists a positive constant κ such that

$$\|d_t u_h^{n+1}\|_0^2 + k\nu \sum_{i=0}^{n+1} \|\nabla d_t u_h^i\|_0^2 \leqslant \kappa, \quad 0 \leqslant n < N.$$

Proof
The proof will be similar to the procedure provided in [18]. Here, we omit it. □

We have the following stability results.

DOI: 10.1002/fld

Theorem 3.5
The solution of Method III has the following estimates:

$$\|u_h^n\|_0^2 + k\nu \sum_{i=0}^{n} \left(\|\nabla u_h^i\|_0^2 + \|p_h^i\|_0^2\right) \leqslant \kappa, \quad 0 \leqslant n \leqslant N,$$

where κ depends only on (n, t, u_0).

Proof
We use the induction argument to establish the stability theorem. Firstly, we assume that

$$k \sum_{i=0}^{n} \|p_h^i\|_0^2 \leqslant \kappa.$$

In the following work, we present the numerical stability in $(n+1)$ step.

Taking $v = 2ku_h^{n+1}$ in (3.4), we have

$$\|u_h^{n+1}\|_0^2 - \|u_h^n\|_0^2 + \|u_h^{n+1} - u_h^n\|_0^2 + 2k\nu\|\nabla u_h^{n+1}\|_0^2 + 2k\left(u_h^{n+1}, \nabla p_h^n\right) = 2k\left(f^{n+1}, u_h^{n+1}\right). \quad (3.5)$$

Using the Cauchy–Schwarz inequality, we acquire

$$2k|\left(u_h^{n+1}, \nabla p_h^n\right)| \leqslant 2k\|\nabla u_h^{n+1}\|_0\|p_h^n\|_0 \leqslant \frac{k\nu}{2}\|\nabla u_h^{n+1}\|_0^2 + \frac{2k}{\nu}\|p_h^n\|_0^2,$$
$$2k|\left(f^{n+1}, u_h^{n+1}\right)| \leqslant 2k\|f^{n+1}\|_{-1}\|\nabla u_h^{n+1}\|_0 \leqslant \frac{k\nu}{2}\|\nabla u_h^{n+1}\|_0^2 + \frac{2k}{\nu}\|f^{n+1}\|_{-1}^2.$$

Combining the aforementioned estimates with (3.5), we obtain

$$\|u_h^{n+1}\|_0^2 - \|u_h^n\|_0^2 + \|u_h^{n+1} - u_h^n\|_0^2 + k\nu\|\nabla u_h^{n+1}\|_0^2 \leqslant \frac{2k}{\nu}\|p_h^n\|_0^2 + \frac{2k}{\nu}\|f^{n+1}\|_{-1}^2.$$

Summing the aforementioned inequalities for each n leads to

$$\|u_h^{n+1}\|_0^2 - \|u_h^0\|_0^2 + k\nu \sum_{i=0}^{n} \|\nabla u_h^{i+1}\|_0^2 \leqslant \frac{k}{\nu} \sum_{i=0}^{n+1} \left(\|p_h^i\|_0^2 + \|f^{i+1}\|_{-1}^2\right).$$

Applying the induction argument, we have

$$\|u_h^{n+1}\|_0^2 + k\nu \sum_{i=0}^{n} \|\nabla u_h^{i+1}\|_0^2 \leqslant \kappa. \quad (3.6)$$

The inequality mentioned previously implies the stability of the velocity. For the stability of the pressure, we have the following estimates.

Taking $q = p_h^{n+1} - p_h^n + \nu\nabla \cdot u_h^{n+1} \triangleq \psi_h^{n+1}$ in (3.3), we obtain

$$\begin{aligned} \|\nabla\psi_h^{n+1}\|_0^2 &= \left(d_t u_h^{n+1}, \nabla\psi_h^{n+1}\right) \leqslant \|d_t u_h^{n+1}\|_0\|\nabla\psi_h^{n+1}\|_0 \\ &\leqslant \frac{1}{2}\|\nabla\psi_h^{n+1}\|_0^2 + \frac{1}{2}\|d_t u_h^{n+1}\|_0^2. \end{aligned} \quad (3.7)$$

DOI: 10.1002/fld

The equation $\psi_h^{n+1} = p_h^{n+1} - p_h^n + \nu\nabla\cdot u_h^{n+1}$ takes inner product with $2p_h^{n+1}$; there holds

$$\begin{aligned}
&\|p_h^{n+1}\|_0^2 - \|p_h^n\|_0^2 + \|p_h^{n+1} - p_h^n\|_0^2 = 2\left(\psi_h^{n+1}, p_h^{n+1}\right) - 2\nu\left(\nabla\cdot u_h^{n+1}, p_h^{n+1}\right)\\
&= 2\left(\psi_h^{n+1}, p_h^{n+1} - p_h^n\right) + 2\left(\psi_h^{n+1}, p_h^n\right) - 2\nu\left(\nabla\cdot u_h^{n+1}, p_h^{n+1} - p_h^n\right)\\
&\quad - 2\nu\left(\nabla\cdot u_h^{n+1}, p_h^n\right).
\end{aligned} \tag{3.8}$$

Using the Cauchy–Schwarz inequality and noticing $\|\nabla\cdot u_h^{n+1}\|_0 \leqslant \|\nabla u_h^{n+1}\|_0$, we obtain

$$\begin{aligned}
2|\left(\psi_h^{n+1}, p_h^{n+1} - p_h^n\right)| &\leqslant \frac{1}{2}\|p_h^{n+1} - p_h^n\|_0^2 + 2\|\psi_h^{n+1}\|_0^2,\\
2|\left(\psi_h^{n+1}, p_h^n\right)| &\leqslant \|\psi_h^{n+1}\|_0^2 + \|p_h^n\|_0^2,\\
2\nu|\left(\nabla\cdot u_h^{n+1}, p_h^{n+1} - p_h^n\right)| &\leqslant \frac{1}{2}\|p_h^{n+1} - p_h^n\|_0^2 + 2\nu^2\|\nabla u_h^{n+1}\|_0^2,\\
2\nu|\left(\nabla\cdot u_h^{n+1}, p_h^n\right)| &\leqslant \nu^2\|\nabla u_h^{n+1}\|_0^2 + \|p_h^n\|_0^2.
\end{aligned}$$

We derive from (3.8) and the aforementioned estimates that

$$\|p_h^{n+1}\|_0^2 \leqslant 3\|p_h^n\|_0^2 + 3\|\psi_h^{n+1}\|_0^2 + 3\nu^2\|\nabla u_h^{n+1}\|_0^2.$$

The aforementioned inequality multiplies k and sums for each n, noticing (3.7); there holds

$$k\sum_{i=0}^{n+1}\|p_h^i\|_0^2 \leqslant 3k\sum_{i=0}^{n}\left(\|p_h^i\|_0^2 + \|d_t u_h^{i+1}\|_0^2 + \nu^2\|\nabla u_h^{i+1}\|_0^2\right).$$

The combination of (3.6) and Lemma 3.2 fulfills the proof. □

Before presenting the error estimates of Method III, for $0 \leqslant n < N$, we denote

$$\begin{aligned}
u(t_{n+1}) &= u^{n+1} = P_h u^{n+1} + (I - P_h)u^{n+1} = U^{n+1} + W^{n+1},\\
U^{n+1} &= P_h u^{n+1}, \quad W^{n+1} = (I - P_h)u^{n+1},\\
e_h^{n+1} &= U^{n+1} - u_h^{n+1}, \quad p(t_{n+1}) = p^{n+1}, \quad \eta_h^{n+1} = p^{n+1} - p_h^{n+1}.
\end{aligned}$$

Similarly to Lemma 3.2, before giving the error estimates, we first have the following lemma. We also leave its proof to the interested readers.

Lemma 3.3
Under the conditions of Theorem 3.5, the following results hold

$$\|d_t e_h^{n+1}\|_0^2 + k\nu\sum_{i=0}^{n+1}\|\nabla d_t e_h^i\|_0^2 \leqslant \kappa\left(H^6 L_h^2 + h^4 + k^2\right).$$

Then we have the following error estimates of Method III.

Theorem 3.6
The convergence results of Method III are

$$\|u(t_n) - u_h^n\|_0^2 + k\nu\sum_{i=0}^{n}\left(\|\nabla u(t_i) - \nabla u_h^i\|_0^2 + \|p(t_i) - p_h^i\|_0^2\right) \leqslant \kappa\left(H^6 L_h^2 + h^4 + k^2\right), \quad 0 \leqslant n \leqslant N,$$

where κ depends only on (n, t, u_0).

DOI: 10.1002/fld

Proof
We also apply the induction arguments to obtain the convergence results. Firstly, we assume that the following estimates are valid:

$$k\sum_{i=0}^{n}\|\eta_h^i\|_0^2 \leqslant \kappa\left(H^6L_h^2+h^4+k^2\right).$$

Subtracting (3.4) from (2.1) at $t=t_{n+1}$, we have

$$\begin{aligned}\left(d_te_h^{n+1},v\right)+\nu a\left(e_h^{n+1},v\right)+b\left(U^{n+1},e_h^{n+1},v\right)+b\left(e_h^{n+1},u_h^{n+1},v\right)+b\left(\hat{u}_h^{n+1},u_h^{n+1},v\right)\\ +kQ^{n+1}(v)+k\left(v,\nabla d_tp^{n+1}\right)+\left(v,\nabla\eta_h^n\right)=\left(g^{n+1},v\right),\quad \forall v\in X_h,\end{aligned}\tag{3.9}$$

where

$$\begin{aligned}\hat{u}_h^{n+1}&=u_h^{n+1}-u_H^{n+1},\quad g^{n+1}=\frac{1}{k}\int_{t_n}^{t_{n+1}}(u(t)-u_t(t_{n+1}))\mathrm{dt},\\ Q^{n+1}(v)&=b\left(U^{n+1},W^{n+1},v\right)+b\left(W^{n+1},U^{n+1},v\right)+b\left(W^{n+1},W^{n+1},v\right).\end{aligned}$$

Taking $v=2ke_h^{n+1}$ in (3.9), we have

$$\begin{aligned}\|e_h^{n+1}\|_0^2-\|e_h^n\|_0^2+\|e_h^{n+1}-e_h^n\|_0^2+2k\nu\|\nabla e_h^{n+1}\|_0^2+2kb(U^{n+1},e_h^{n+1},e_h^{n+1})\\ +2kb\left(e_h^{n+1},u_h^{n+1},e_h^{n+1}\right)+2kb\left(\hat{u}_h^{n+1},u_h^{n+1},e_h^{n+1}\right)+2kQ^{n+1}\left(e_h^{n+1}\right)\\ +2k^2\left(e_h^{n+1},\nabla d_tp^{n+1}\right)+2k\left(e_h^{n+1},\nabla\eta_h^n\right)=2k\left(g^{n+1},e_h^{n+1}\right).\end{aligned}\tag{3.10}$$

Using (2.3), (2.4), and (2.5), there hold

$$\begin{aligned}2k|b\left(e_h^{n+1},u_h^{n+1},e_h^{n+1}\right)|&\leqslant 2c_0kL_h\|\nabla u_h^{n+1}\|_0\|\nabla e_h^{n+1}\|_0\|e_h^{n+1}\|_0\\ &\leqslant\frac{k\nu}{6}\|\nabla e_h^{n+1}\|_0^2+\frac{6c_0^2kL_h^2}{\nu}\|e_h^{n+1}\|_0^2\|\nabla u_h^{n+1}\|_0^2,\\ 2k|b\left(\hat{u}_h^{n+1},u_h^{n+1},e_h^{n+1}\right)|&\leqslant 2c_0kL_h\|\hat{u}_h^{n+1}\|_0\|\nabla u_h^{n+1}\|_0\|\nabla e_h^{n+1}\|_0\\ &\leqslant\frac{k\nu}{6}\|\nabla e_h^{n+1}\|_0^2+\frac{6c_0^2kL_h^2}{\nu}\|\hat{u}_h^{n+1}\|_0^2\|\nabla u_h^{n+1}\|_0^2,\\ 2k|Q^{n+1}\left(e_h^{n+1}\right)|&\leqslant 6c_0k\|U^{n+1}\|_2\|W^{n+1}\|_0\|\nabla e_h^{n+1}\|_0\\ &\leqslant\frac{k\nu}{6}\|\nabla e_h^{n+1}\|_0^2+\frac{6c_0^2k}{\nu}\|U^{n+1}\|_2^2\|W^{n+1}\|_0^2,\\ 2k^2|\left(e_h^{n+1},\nabla d_tp^{n+1}\right)|&\leqslant 2k^2\|\nabla e_h^{n+1}\|_0\|d_tp^{n+1}\|_0\leqslant\frac{k\nu}{6}\|\nabla e_h^{n+1}\|_0^2+\frac{6k^3}{\nu}\|d_tp^{n+1}\|_0^2,\\ 2k|\left(e_h^{n+1},\nabla\eta_h^n\right)|&\leqslant 2k\|\nabla e_h^{n+1}\|_0\|\eta_h^n\|_0\leqslant\frac{k\nu}{6}\|\nabla e_h^{n+1}\|_0^2+\frac{6k}{\nu}\|\eta_h^n\|_0^2,\\ 2k|\left(g^{n+1},e_h^{n+1}\right)|&\leqslant 2k\|\nabla e_h^{n+1}\|_0\|g^{n+1}\|_{-1}\leqslant\frac{k\nu}{6}\|\nabla e_h^{n+1}\|_0^2+\frac{6k}{\nu}\|g^{n+1}\|_{-1}^2.\end{aligned}$$

The combination of (3.10) and the aforementioned estimates admits

$$\begin{aligned}\|e_h^{n+1}\|_0^2-\|e_h^n\|_0^2+\|e_h^{n+1}-e_h^n\|_0^2+k\nu\|\nabla e_h^{n+1}\|_0^2\leqslant\frac{6k}{\nu}\left(c_0^2L_h^2\|e_h^{n+1}\|_0^2\|\nabla u_h^{n+1}\|_0^2\right.\\ \left.+c_0^2L_h^2\|\hat{u}_h^{n+1}\|_0^2\|\nabla u_h^{n+1}\|_0^2+c_0^2\|U^{n+1}\|_2^2\|W^{n+1}\|_0^2+k^2\|d_tp^{n+1}\|_0^2+\|\eta_h^n\|_0^2+\|g^{n+1}\|_{-1}^2\right).\end{aligned}$$

DOI: 10.1002/fld

Summing the aforementioned inequality for each n, we have

$$\|e_h^{n+1}\|_0^2 - \|e_h^0\|_0^2 + k\nu \sum_{i=0}^{n} \|\nabla e_h^{i+1}\|_0^2 \leqslant \frac{6k}{\nu} \sum_{i=0}^{n} \big(c_0^2 L_h^2 \|e_h^{i+1}\|_0^2 \|\nabla u_h^{i+1}\|_0^2$$
$$+ c_0^2 L_h^2 \|\hat{u}_h^{i+1}\|_0^2 \|\nabla u_h^{i+1}\|_0^2 + c_0^2 \|U^{i+1}\|_2^2 \|W^{i+1}\|_0^2 + k^2 \|d_t p^{i+1}\|_0^2 + \|\eta_h^i\|_0^2 + \|g^{i+1}\|_{-1}^2\big).$$

Applying Gronwall Lemma 3.1 to the aforementioned inequality and noticing (3.1), we have

$$\|e_h^{n+1}\|_0^2 + k\nu \sum_{i=0}^{n} \|\nabla e_h^{i+1}\|_0^2 \leqslant \kappa \left(H^6 L_h^2 + h^4 + k^2\right). \tag{3.11}$$

Then we give the error estimates of the pressure.

Adding some zero terms to (3.3), we acquire

$$\left(\nabla \phi_h^{n+1}, \nabla q\right) = \left(d_t e_h^{n+1}, \nabla q\right) + k\left(\nabla d_t p^{n+1}, \nabla q\right), \quad \forall q \in M_h. \tag{3.12}$$

It follows from the aforementioned equation that

$$\left(\nabla d_t \phi_h^{n+1}, \nabla q\right) = \left(d_{tt} e_h^{n+1}, \nabla q\right) + k\left(\nabla d_{tt} p^{n+1}, \nabla q\right), \quad \forall q \in M_h.$$

Taking $q = \eta_h^{n+1} - \eta_h^n + \nu \nabla \cdot e_h^{n+1} \triangleq \phi_h^{n+1}$ in (3.12), we have

$$\begin{aligned} \|\nabla \phi_h^{n+1}\|_0^2 &= \left(d_t e_h^{n+1}, \nabla \phi_h^{n+1}\right) + k\left(\nabla d_t p^{n+1}, \nabla \phi_h^{n+1}\right) \\ &\leqslant \|d_t e_h^{n+1}\|_0 \|\nabla \phi_h^{n+1}\|_0 + k\|\nabla d_t p^{n+1}\|_0 \|\nabla \phi_h^{n+1}\|_0 \\ &\leqslant \frac{1}{2}\|\nabla \phi_h^{n+1}\|_0^2 + \|d_t e_h^{n+1}\|_0^2 + k^2 \|\nabla d_t p^{n+1}\|_0^2. \end{aligned} \tag{3.13}$$

The equation $\phi_h^{n+1} = \eta_h^{n+1} - \eta_h^n + \nu \nabla \cdot e_h^{n+1}$ takes the inner product with $2\eta_h^{n+1}$, leading to

$$\begin{aligned} &\|\eta_h^{n+1}\|_0^2 - \|\eta_h^n\|_0^2 + \|\eta_h^{n+1} - \eta_h^n\|_0^2 = 2\left(\phi_h^{n+1}, \eta_h^{n+1}\right) - 2\nu\left(\nabla \cdot e_h^{n+1}, \eta_h^{n+1}\right) \\ &= 2\left(\phi_h^{n+1}, \eta_h^{n+1} - \eta_h^n\right) + 2\left(\phi_h^{n+1}, \eta_h^n\right) - 2\nu\left(\nabla \cdot e_h^{n+1}, \eta_h^{n+1} - \eta_h^n\right) - 2\nu\left(\nabla \cdot e_h^{n+1}, \eta_h^n\right). \end{aligned} \tag{3.14}$$

We have the following estimates

$$\begin{aligned} 2|\left(\phi_h^{n+1}, \eta_h^{n+1} - \eta_h^n\right)| &\leqslant \frac{1}{2}\|\eta_h^{n+1} - \eta_h^n\|_0^2 + 2\|\phi_h^{n+1}\|_0^2, \\ 2|\left(\phi_h^{n+1}, \eta_h^n\right)| &\leqslant \|\phi_h^{n+1}\|_0^2 + \|\eta_h^n\|_0^2, \\ 2\nu|\left(\nabla \cdot e_h^{n+1}, \eta_h^{n+1} - \eta_h^n\right)| &\leqslant \frac{1}{2}\|\eta_h^{n+1} - \eta_h^n\|_0^2 + 2\nu^2 \|\nabla e_h^{n+1}\|_0^2, \\ 2\nu|\left(\nabla \cdot e_h^{n+1}, \eta_h^n\right)| &\leqslant \nu^2 \|\nabla e_h^{n+1}\|_0^2 + \|\eta_h^n\|_0^2. \end{aligned}$$

Combining (3.14) with the aforementioned estimates, we obtain

$$\|\eta_h^{n+1}\|_0^2 \leqslant 3\|\eta_h^n\|_0^2 + 3\|\phi_h^{n+1}\|_0^2 + 3\nu^2 \|\nabla e_h^{n+1}\|_0^2.$$

Summing the aforementioned inequality for each n and noticing (3.13), we have

$$k \sum_{i=0}^{n} \|\eta_h^{i+1}\|_0^2 \leqslant 3k \sum_{i=0}^{n} \left(\|\eta_h^i\|_0^2 + 2\|d_t e_h^{i+1}\|_0^2 + 2k^2 \|d_t p^{i+1}\|_0^2 + \nu^2 \|\nabla e_h^{i+1}\|_0^2\right).$$

Noticing (3.11) and Lemma 3.3, we acquire

$$k \sum_{i=0}^{n+1} \|\eta_h^i\|_0^2 \leqslant \kappa \left(H^6 L_h^2 + h^4 + k^2\right).$$

Hence, we obtain the error estimates in the $(n+1)$ step and complete the proof of this theorem. □

DOI: 10.1002/fld

Remark 3.1
For the three kinds of two-level consistent splitting schemes (Methods I, II, and III), we first solve a standard Galerkin method (3.2) in the coarse-level subspace to acquire the large eddy components (u_H^n, p_H^n). As an initial solution, we solve a linear problem in the fine-level subspace based on Stokes, Newton, and Oseen iterations, respectively. Finally, the pressure is updated by solving a Poisson equation (3.3). Step 2 reflects the interaction between the large and small eddy components. It is easy to find that Stokes iteration is the simplest approximation for the nonlinear term and Newton iteration is the most complicated method, which is the second-order approximation for the nonlinear term. Hence, Method I is the most time-saving method, while Method II can hold the best accuracy among the three methods.

It follows from Theorem 3.2, Theorem 3.4, and Theorem 3.6 to reach the same accuracy as the usual one-level method with the space size h; we should choose $h \sim L_h H^2$ for Method II. While for Methods I and III, the configurations should be $h^2 \sim L_h H^3$. Specifically, if we fix the relation $h \sim H^2$, only Method II can obtain the good approximations. We should choose a finer H to keep the aforementioned configuration for a fixed h by Methods I and III if we want to improve the accuracy.

Remark 3.2
The detailed proof of Theorem 3.3 and Theorem 3.4 can be found in [18]. The stability and convergence results of Methods I and III are exhibited in Theorem 3.1, Theorem 3.2, Theorem 3.5, and Theorem 3.6. The proof of these theorems will be similar to the procedure in [18]. Here, we only give the numerical analysis of Method III because it is newly proposed in this paper. Also, we find that the constant κ in Theorem 3.1 and Theorem 3.3 is proportional to the time t and has an exponential factor with respect to $\frac{1}{\nu}$, owing to the applications of Gronwall lemma. Therefore, κ will increase rapidly when ν decreases at some time. On the other hand, when we try to acquire the stability of Method III, we take $v = u_h^{n+1}$ in (3.4) as the usual way; the term $b(u_H^{n+1}, u_h^{n+1}, u_h^{n+1})$ will be zero. Hence, we can acquire the stability of Method III without using the Gronwall lemma. Specifically, the constant κ in Theorem 3.5 is independent of ν. In other words, Method III will perform the best for the small viscosity problem among the three methods.

4. NUMERICAL EXAMPLES

This section gives some numerical examples to illustrate the performance of the three kinds of two-level consistent splitting schemes. We choose the well-known Taylor–Hood element in all examples. That is, the Lagrange quadratic elements are used to approximate the velocity and line elements to approximate the pressure. For all the implicit time stepping in the simulations, we use Newton iteration with tolerance 10^{-6}. And we use the generalized minimal residual iterative method to solve the linear algebraic equations arising at every time step with tolerance 10^{-9}. All numerical experiments are carried out on a Pentium(R) Dual-Core CPU E5500 with 2-GB memory, under the Debian GNU/Linux operating system, with the FreeFem++ package [29] compilers.

4.1. Analytical solution

We compare the accuracy of the three kinds of two-level consistent splitting schemes with a known analytical solution. The prescribed solution is given by

$$\begin{cases} u_1(x, y, t) = \pi \sin t \sin 2\pi y \sin^2 \pi x, \\ u_2(x, y, t) = -\pi \sin t \sin 2\pi x \sin^2 \pi y, \\ p(x, y, t) = \sin t \cos \pi x \sin \pi y. \end{cases}$$

The right-hand f is determined such that (u_1, u_2, p) is the solution of the Navier–Stokes equation (1.1).

DOI: 10.1002/fld

We first fix the time step size $k = 0.001$, the final time $T = 1$, and $\nu = 1$. We choose the configuration $h \sim H^2$ of the fine mesh size h and coarse mesh size H to acquire the accuracy of the three methods. The advantage of two-level methods in CPU time in comparison with the one-level methods is presented in Tables I and II. We can see the two-level methods can acquire the same accuracy as the one-level methods with a proper coarse method size H. In all the tables,

$$\|e_u\|_{L^\infty(0,T;Y)} = \max_{0\leqslant i\leqslant N} \frac{\|u(t_i) - u_h^i\|_0}{\|u(t_i)\|_0}, \quad \|e_u\|_{L^2(0,T;X)} = \left(k\sum_{i=0}^{N} \frac{\|u(t_i) - u_h^i\|_1^2}{\|u(t_i)\|_1^2}\right)^{\frac{1}{2}},$$

$$\|e_p\|_{L^2(0,T;Y)} = \left(k\sum_{i=0}^{N} \frac{\|p(t_i) - p_h^i\|_0^2}{\|p(t_i)\|_0^2}\right)^{\frac{1}{2}}, \quad \|e_p\|_{L^\infty(0,T;X)} = \max_{0\leqslant i\leqslant N} \frac{\|p(t_i) - p_h^i\|_1}{\|p(t_i)\|_1}.$$

Furthermore, Tables III–V report the corresponding results of Methods I, II, and III, respectively. Just like Remark 3.1, Method I is the most time-saving method among the three methods. Method II has the better convergence order than Methods I and III.

To establish the possible impact of the viscosity on the three methods, we present the pressure contours of the three methods for $\nu = 0.1$ and $\nu = 0.001$. In Figures 1–3, we fix the time step size $k = 0.001$ and choose the coarse mesh size $H = 1/16$ and the fine mesh size $h = 1/32$. For $\nu = 0.1$, which is the large viscosity problem, the three methods all can give the good approximations at $t = 2$ (Figure 1). For the further small viscosity $\nu = 0.001$, Method I appears oscillations at $t = 1.2$, while the other two methods can still keep the good approximations (Figure 2). For the long-time simulations, Method II also appears oscillations at $t = 2$; only Method III can provide a good accuracy even at $t = 2$ (Figure 3). The velocity contours will present the same results as the pressure contours by using the three methods. Here, we only give the pressure contours to save the place of this paper.

4.2. The flow around a circular cylinder

Another example to be considered here is the flow around a circular cylinder, which is one of the classical flow problems. At upper and lower computational boundaries and at the inflow section, a uniform free-stream velocity boundary condition is imposed. The traction-free condition is imposed at the outflow boundary. The geometry and the boundary conditions of the cylinder problem are shown in Figure 4. The coarse and fine meshes are listed in Figure 5. We simulate this problem for $T = 500$ and choose the time step size $k = 0.05$.

The cylinder problem can be characterized by the Reynolds number, which is based on the maximum velocity $u_{\max}$ and the cylinder diameter d, i.e., $Re = (u_{\max}d)/\nu$. For Reynolds number $Re \leqslant 40$ when the flow is steady, a wake behind the cylinder develops. The wake is two symmetrical eddies upstream and downstream and will become bigger with the increasing of the Reynolds numbers. For Reynolds number $Re > 40$, the flow is unsteady, causing periodic wake flow with vortex shedding behind the cylinder. It is the well-known Karman vortex street. Vortex shedding occurs at a well-defined frequency.

Figures 6–8 present the pressure contours of the three methods with different Reynolds numbers. Just like the first example, for the small Reynolds number $Re = 40$, the three methods all can give the good approximations at $t = 20$ (Figure 6). For the further large Reynolds number $Re = 80$, Method I appears oscillations, while the other two methods can still keep the good approximations (Figure 7). With the increasing of Reynolds number $Re = 2500$, Method I diverges at $t = 1.05$, Method II also appears oscillations at $t = 20$, and only Method III can perform well at $t = 20$ (Figure 8).

Having demonstrated the performances of the three methods, the focus of this numerical example is to demonstrate the results of Oseen correction because we have given many numerical results of the Stokes correction in [17] and the Newton correction in [18]. For the additionally proposed two-level consistent splitting schemes based on Oseen correction, we discuss the long-time performance

DOI: 10.1002/fld

Table I. Results of one-level method.

h	$\|e_u\|_{L^\infty(0,T;Y)}$	Order	$\|e_u\|_{L^2(0,T;X)}$	Order	$\|e_p\|_{L^2(0,T;Y)}$	Order	$\|e_p\|_{L^\infty(0,T;X)}$	Order	CPU time
1/16	0.000608993		0.0112695		0.00557182		0.102407		1241.6s
1/25	0.000161046	2.9804	0.00464387	1.9865	0.00159174	2.8074	0.0623799	1.1108	1957.1s
1/36	5.51200e-05	2.9403	0.00224451	1.9939	0.000680748	2.3294	0.0428216	1.0317	3786.6s
1/49	2.37553e-05	2.7301	0.00121272	1.9968	0.000361541	2.0526	0.0313504	1.0114	5913.2s

DOI: 10.1002/fld

Table II. Results of two-level method.

H	h	$\|e_u\|_{L^\infty(0,T;Y)}$	Order	$\|e_u\|_{L^2(0,T;X)}$	Order	$\|e_p\|_{L^2(0,T;Y)}$	Order	$\|e_p\|_{L^\infty(0,T;X)}$	Order	CPU time
1/4	1/16	0.00060923		0.0112696		0.00709884		0.108232		953.4s
1/5	1/25	0.000161092	2.9806	0.00464389	1.9865	0.0020956	2.7339	0.0638619	1.1821	1438.8s
1/6	1/36	5.51431e-05	2.9400	0.00224451	1.9939	0.000873435	2.4000	0.0432947	1.0660	2390.5s
1/7	1/49	2.37692e-05	2.7296	0.00121272	1.9968	0.000444879	2.1882	0.0315237	1.0292	4055.8s

DOI: 10.1002/fld

Table III. Results of Method I.

H	h	$\|e_u\|_{L^\infty(0,T;Y)}$	Order	$\|e_u\|_{L^2(0,T;X)}$	Order	$\|e_p\|_{L^2(0,T;Y)}$	Order	$\|e_p\|_{L^\infty(0,T;X)}$	Order	CPU time
1/4	1/16	0.00166363		0.0120046		0.0680661		0.764246		677.3s
1/5	1/25	0.000675108	2.0209	0.00513168	1.9043	0.0354272	1.4632	0.487916	1.0055	953.4s
1/6	1/36	0.000339489	1.8852	0.00261187	1.8521	0.0216961	1.3447	0.348764	0.9208	1428.1s
1/7	1/49	0.000191276	1.8609	0.00149678	1.8059	0.0143703	1.3363	0.260683	0.9442	2268.5s

DOI: 10.1002/fld

Table IV. Results of Method II.

H	h	$\|e_u\|_{L^\infty(0,T;Y)}$	Order	$\|e_u\|_{L^2(0,T;X)}$	Order	$\|e_p\|_{L^2(0,T;Y)}$	Order	$\|e_p\|_{L^\infty(0,T;X)}$	Order	CPU time
1/4	1/16	0.000684678		0.0112712		0.00728561		0.107388		704.4s
1/5	1/25	0.000203204	2.7219	0.00464464	1.9865	0.00245014	2.4418	0.0637287	1.1692	1033.9s
1/6	1/36	8.13279e-05	2.5113	0.0022449	1.9939	0.00113491	2.1105	0.0432713	1.0617	1626.7s
1/7	1/49	4.16016e-05	2.1743	0.00121299	1.9967	0.000688596	1.6207	0.0315263	1.0271	2607.3s

DOI: 10.1002/fld

Table V. Results of Method III.

H	h	$\|e_u\|_{L^\infty(0,T;Y)}$	Order	$\|e_u\|_{L^2(0,T;X)}$	Order	$\|e_p\|_{L^2(0,T;Y)}$	Order	$\|e_p\|_{L^\infty(0,T;X)}$	Order	CPU time
1/4	1/16	0.000632544		0.0112783		0.0268662		0.195204		696.3s
1/5	1/25	0.000194657	2.6407	0.00465117	1.9847	0.0121193	1.7838	0.120365	1.0834	993.1s
1/6	1/36	9.18565e-05	2.0596	0.00224986	1.9917	0.00635052	1.7723	0.0752099	1.2896	1524.7s
1/7	1/49	6.81212e-05	0.9696	0.0012178	1.9910	0.00399944	1.4998	0.0508025	1.2726	2420.5s

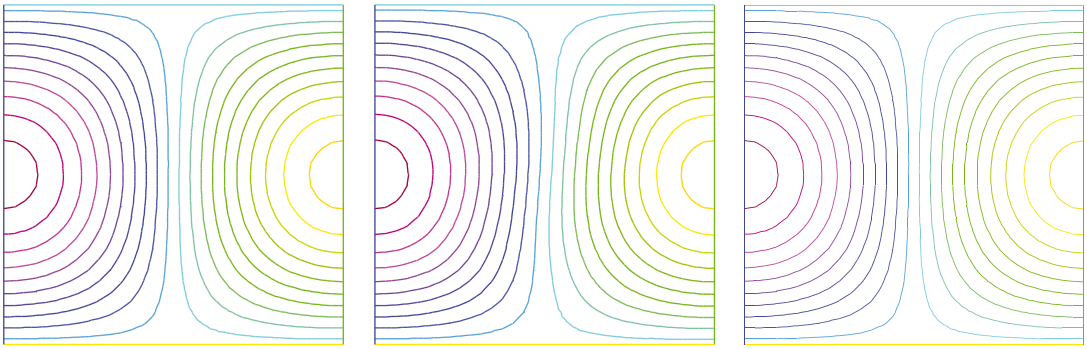

(a) Method I (b) Method II (c) Method III

Figure 1. Pressure contours of (a) Methods I, (b) II, and (c) III for $\nu = 0.1$ at $t = 2$.

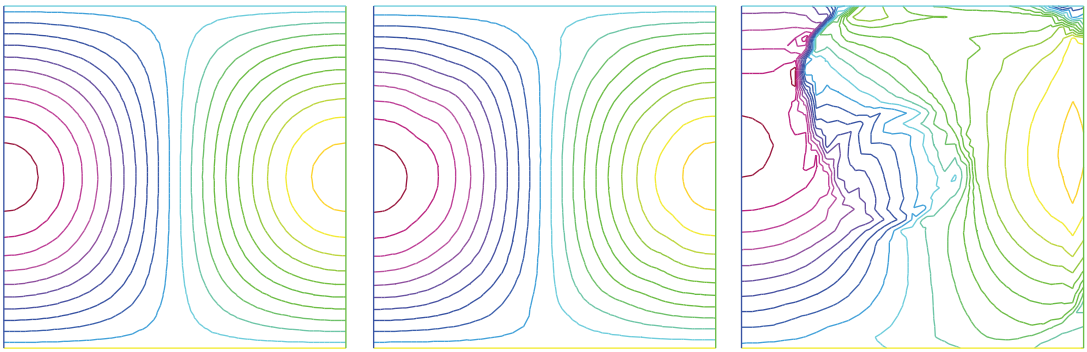

(a) Method I (b) Method II (c) Method III

Figure 2. Pressure contours of (a) Methods I, (b) II, and (c) III for $\nu = 0.001$ at $t = 1.2$.

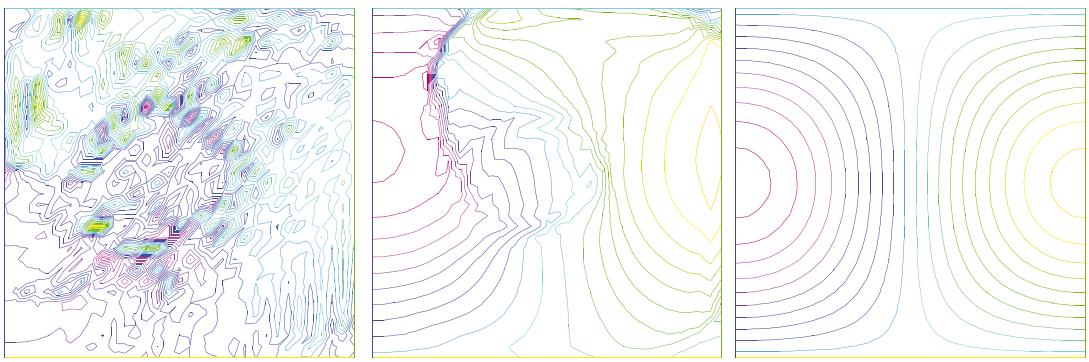

(a) Method I (b) Method II (c) Method III

Figure 3. Pressure contours of (a) Methods I, (b) II, and (c) III for $\nu = 0.001$ at $t = 2$.

of Method III furthermore. For the long-time behavior, Figures 9–11 present the contours of the streamlines, pressure, and vorticity for $Re = 40$ and $Re = 80$ at $t = 500$, respectively. These figures show the features of the steady and unsteady cases mentioned earlier very well. Figure 12 shows the temporal development of the drag and lift coefficients. This figure shows that the flow field is well developed and has reached an unsteady periodic behavior about from $t = 350$. This figure also illustrates the shedding period $T_p = 24.5$. Furthermore, Figure 13 provides the streamlines for $Re = 80$ at $t = 450$ and $t = 474.5$. These two streamlines are almost the same. Moreover, some comparisons of the drag coefficients C_D, the wake length L_r/d that is from the rearmost point of the

DOI: 10.1002/fld

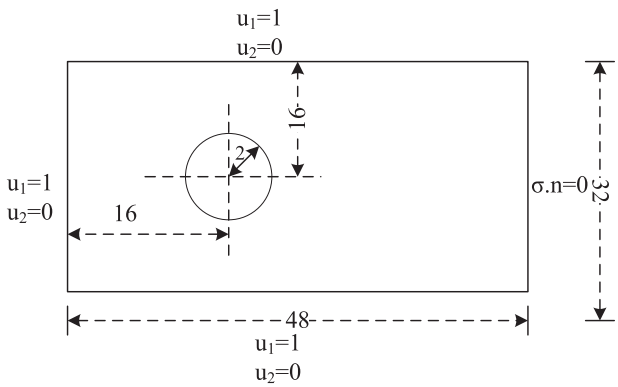

Figure 4. The statement of the flow around a cylinder.

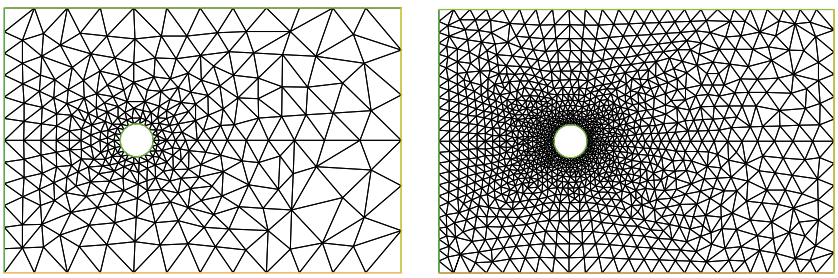

(a) 602 elements (b) 2406 elements

Figure 5. (a) Coarse and (b) fine meshes.

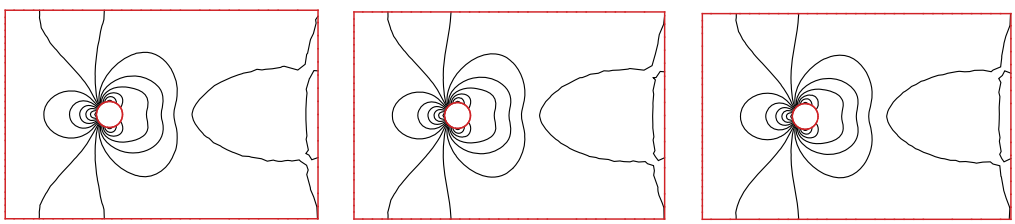

(a) Method I (b) Method II (c) Method III

Figure 6. Pressure contours of (a) Methods I, (b) II, and (c) III for $Re = 40$ at $t = 20$.

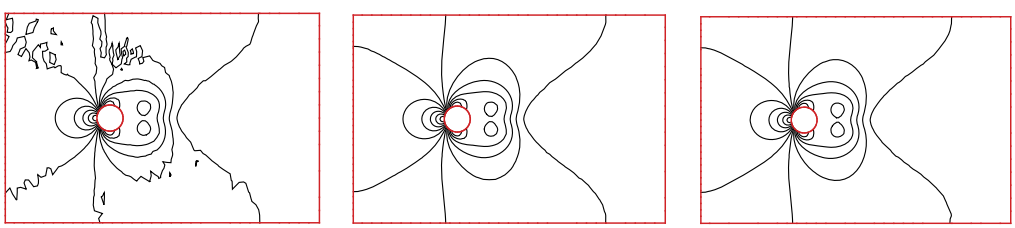

(a) Method I (b) Method II (c) Method III

Figure 7. Pressure contours of (a) Methods I, (b) II, and (c) III for $Re = 80$ at $t = 20$.

DOI: 10.1002/fld

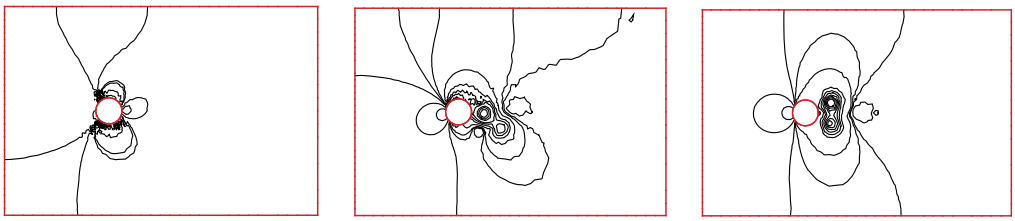

(a) Method I ($t = 1$) (b) Method II ($t = 20$) (c) Method III ($t = 20$)

Figure 8. Pressure contours of (a) Methods I, (b) II, and (c) III for $Re = 2500$.

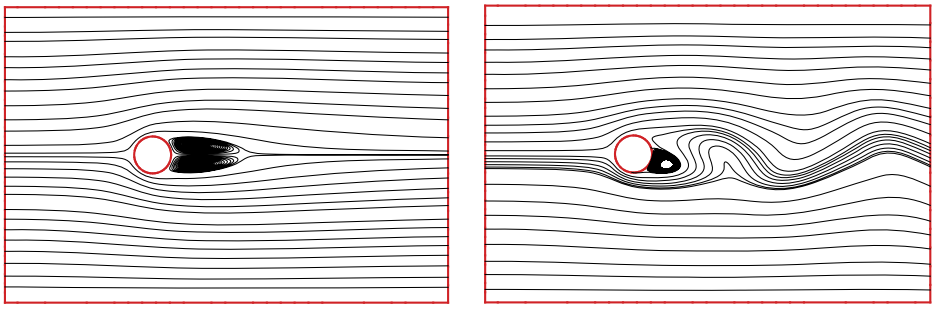

(a) Re=40 (b) Re=80

Figure 9. Streamlines for (a) $Re = 40$ and (b) $Re = 80$ at $t = 500$.

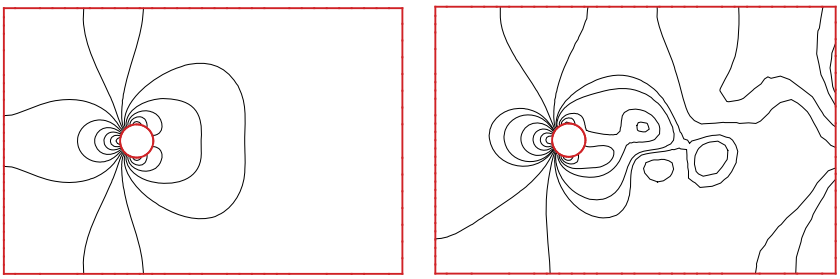

(a) Re=40 (b) Re=80

Figure 10. Pressure contours for (a) $Re = 40$ and (b) $Re = 80$ at $t = 500$.

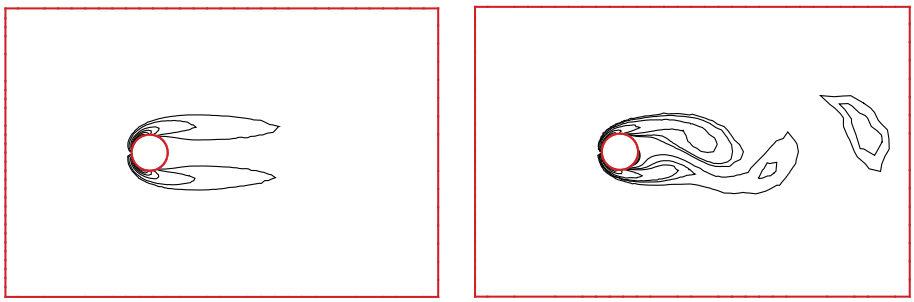

(a) Re=40 (b) Re=80

Figure 11. Vorticity contours for (a) $Re = 40$ and (b) $Re = 80$ at $t = 500$.

DOI: 10.1002/fld

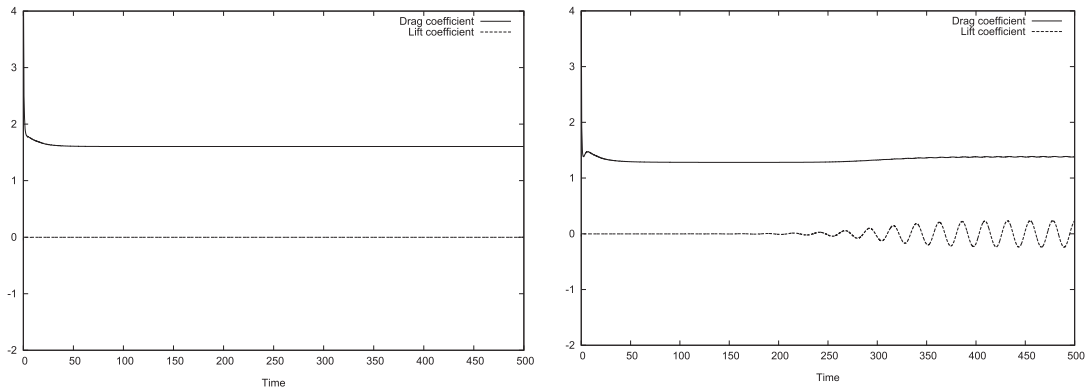

(a) Re=40 (b) Re=80

Figure 12. Drag and lift coefficients for (a) $Re = 40$ and (b) $Re = 80$.

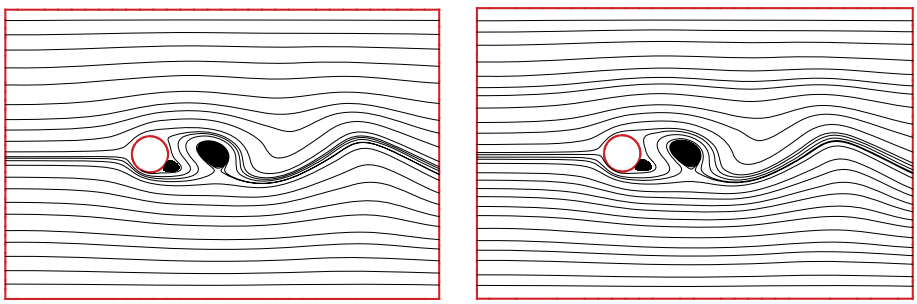

(a) t=450 (b) t=474.5

Figure 13. Streamlines for $Re = 80$ at (a) $t = 450$ and (b) $t = 474.5$.

Table VI. The comparisons of the drag coefficients, the wake length, the separation angle, and the Strouhal number.

	$Re = 40$			$Re = 80$	
Method	C_D	L_r/d	θ	C_D	S_t
Dennis [30]	1.522	2.35	53.8	—	—
Ding [31]	1.713	2.20	53.5	—	—
Russell [32]	1.60	2.29	53.1	—	—
Ye [33]	1.52	2.27	—	1.37	0.15
Silva [34]	1.54	—	—	1.40	0.15
Present work	1.60	2.26	53.5	1.38	0.16

cylinder to the end of the wake, the separation angle θ, and the Strouhal number $St = d/(u_{\max}T_p)$ with some previous simulations are listed in Table VI, which shows that our results can agree well with the results of previous studies.

5. CONCLUSIONS

In this paper, we have studied three kinds of fully discrete two-level consistent splitting methods for the time-dependent Navier–Stokes equations. Methods I and II are proposed in the preceding papers [17, 18]. We additionally propose a two-level consistent splitting schemes based on Oseen correction (Method III) for the large Reynolds number problems and the long-time simulations. The detailed stability and convergence results of Method III are given. Some numerical results are shown for the time-dependent Navier–Stokes equations by using three kinds of two-level consistent splitting

DOI: 10.1002/fld

schemes. The first example is a test problem to see the convergence orders, and the other is the flow past a circular cylinder. The Stokes, Newton, and Oseen iterations reflect the interaction between large and small eddy components. For large viscosity case, Stokes correction method (Method I) is a good choice. For the moderate viscosity case, Newton correction method (Method II) can acquire the best accuracy. For the small viscosity case, Oseen correction method (Method III) is preferable for the long-time simulations.

For the numerical examples, we only consider the two-dimensional Navier–Stokes equations for simplicity. A similar idea can be applied in a straightforward way to the three-dimensional case according to our analysis. In this paper, our main interest is to compare the three kinds of two-level consistent splitting schemes for the time-dependent Navier–Stokes equations. These methods are only an interesting first step. We will give the numerical examples in high-dimensional cases in our future work.

ACKNOWLEDGEMENTS

The work was subsidized by the NSF of China (grant nos 51236006 and 11401466), China Postdoctoral Science Foundation (grant no. 2013M540750), and the PhD Programs Foundation of Ministry of Education of China (grant no. 20130201120052).

REFERENCES

1. Chorin A. Numerical solution of the Navier–Stokes equations. *Mathematics of Computation* 1968; **22**(104):745–762.
2. Temam R. Sur I'approximation de la solution des equations de Navier–Stokes par la methode des pas fractionnaires ii. *Archive for Rational Mechanics and Analysis* 1969; **32**(2):135–153.
3. Guermond J, Shen J. Velocity-correction projection methods for incompressible flows. *SIAM Journal on Numerical Analysis* 2003; **41**(1):112–134.
4. Guermond J, Shen J. A new class of truly consistent splitting schemes for incompressible flows. *Journal of Computational Physics* 2003; **192**(1):262–276.
5. Guermond J, Minev P, Shen J. An overview of projection methods for incompressible flows. *Computer Methods in Applied Mechanics and Engineering* 2006; **195**(44-47):6011–6045.
6. Shen J, Yang X. Error estimates for finite element approximations of consistent splitting schemes for incompressible flows. *Discrete and Continuous Dynamical Systems-Series B* 2007; **8**(3):663–676.
7. Xu J. Two-grid finite element discretization technique for linear and nonlinear PDEs. *SIAM Journal on Numerical Analysis* 1996; **33**(5):1759–1777.
8. Mu M, Xu J. A two-grid method of a mixed Stokes–Darcy model for coupling fluid flow with porous media flow. *SIAM Journal on Numerical Analysis* 2007; **45**(5):1801–1813.
9. Cao M, Mu M, Xu J. Numerical solution to a mixed Navier–Stokes/Darcy model by the two-grid approach. *SIAM Journal on Numerical Analysis* 2009; **47**(5):3325–3338.
10. Layton W. A two-level method with backtracking for the Navier–Stokes equations. *SIAM Journal on Numerical Analysis* 1998; **35**(5):2035–2054.
11. Ayuso B, Garciá-Archilla B, Novo J. The postprocessed mixed finite element method for the Navier–Stokes equations. *SIAM Journal on Numerical Analysis* 2005; **43**(3):1091–1111.
12. Frutos J, Garcia-Archilla B, Novo J. Optimal error bounds for two grid schemes applied to the Navier–Stokes equations. *Applied Mathematics and Computation* 2012; **218**(13):7034–7051.
13. Liu Q, Hou Y. A postprocessing mixed finite element method for the Navier–Stokes equations. *International Journal of Computational Fluid Dynamics* 2009; **23**(6):461–475.
14. Liu Q, Hou Y. A two-level defect-correction mehod for Navier–Stokes equations. *Bulletin of the Australian Mathematical Society* 2010; **81**(3):442–454.
15. Liu Q, Hou Y. A two-level finite element method for the Navier–Stokes equations based on a new projection. *Applied Mathematical Modelling* 2010; **34**(2):383–399.
16. Liu Q, Hou Y, Liu Q. A two-level method in time and space for solving the Navier–Stokes equations based on Newton iteration. *Computers & Mathematics with Applications* 2012; **64**(11):3569–3579.
17. Liu Q, Hou Y, Wang Z, Zhao J. A two-level consistent splitting scheme for the Navier–Stokes equations, submitted.
18. Liu Q, Hou Y, Wang Z, Zhao J. Fully discrete two-level consistent splitting method for the Navier–Stokes equations, submitted.
19. Hou Y, Li K. Postprocessing Fourier Galerkin method for the Navier–Stokes equations. *SIAM Journal on Numerical Analysis* 2009; **47**(3):1909–1922.
20. He Y. Two-level method based on finite element and Crank–Nicolson extrapolation for the time-dependent Navier–Stokes equations. *SIAM Journal on Numerical Analysis* 2003; **41**(4):1263–1285.
21. Xu H, He Y. Some iterative finite element methods for steady Navier–Stokes equations with different viscosities. *Journal of Computational Physics* 2013; **232**(1):136–152.

DOI: 10.1002/fld

22. He Y, Li J. Two-level methods based on three corrections for the 2D/3D steady Navier–Stokes equations. *International Journal of Numerical Analysis and Modeling* 2011; **2**(1):42–45.
23. Shang Y. A two-level subgrid stabilized Oseen iterative method for the steady Navier–Stokes equations. *Journal of Computational Physics* 2013; **233**(1):210–226.
24. Shang Y, He Y, Luo Z. A comparison of three kinds of local and parallel finite element algorithms based on two-grid discretizations for the stationary Navier–Stokes equations. *Computers & Fluids* 2011; **40**(1):249–257.
25. Heywood J, Rannacher R. Finite element approximation of the nonstationary Navier–Stokes problems. part I: regularity of solutions and second-order spatial discretization. *SIAM Journal on Numerical Analysis* 1982; **19**(2): 275–311.
26. Heywood J, Rannacher R. Finite element approximation of the nonstationary Navier–Stokes problems. part IV: error estimates for second-order time discretization. *SIAM Journal on Numerical Analysis* 1990; **27**(2):353–384.
27. Brezis H, Gallout T. Nonlinear SchrÃűedinger evolution equations. *Nonlinear Analysis* 1980; **4**(4):667–681.
28. Shen J. Long time stability and convergence for fully discrete nonlinear Galerkin methods. *Applicable Analysis* 1990; **38**(4):201–229.
29. Hecht F. (Available from: www.freefem.org/ff++) [accessed on June 2013].
30. Dennis S, Chang G. Numerical solutions for steady flow past a circular cylinder at Reynolds numbers up to 100. *Journal of Fluid Mechanics* 1970; **42**(3):471–489.
31. Ding H, Shu C, Yeo K, Xu D. Simulation of incompressible viscous flows past a circular cylinder by hybrid FD scheme and meshless least square-based finite difference method. *Computer Methods in Applied Mechanics and Engineering* 2004; **193**(9-11):727–744.
32. Russell D, Wang Z. A cartesian grid method for modeling multiple moving objects in 2D incompressible viscous flow. *Journal of Computational Physics* 2003; **191**(1):177–205.
33. Ye T, Mittal R, Udaykumar H, Shyy W. An accurate Cartesian grid method for viscous incompressible flows with complex immersed boundaries. *Journal of Computational Physics* 1999; **156**(2):209–240.
34. Lima A, Silva E, Silveira-Neto A, Damasceno J. Numerical simulation of two-dimensional flows over a circular cylinder using the immersed boundary method. *Journal of Computational Physics* 2003; **189**(2):351–370.

DOI: 10.1002/fld